

ARTICLE

Open Access

# High-performance co-oscillating electrochemical vector hydrophone based on integrated microelectrodes with microgrooves

Honghao Zhang<sup>1,2</sup>, Yulan Lu<sup>1,2</sup>✉, Jintao Hu<sup>1,2</sup>, Qinghua Liu<sup>1,2</sup>, Wenlang Zhao<sup>1,2</sup>, Hongmin Jiang<sup>1,2</sup>, Maoqi Zhu<sup>1,2</sup>✉, Zhenyu Sun<sup>1,2</sup>, Guangyang Gou<sup>1</sup>, Deyong Chen<sup>1,2</sup>✉ and Junbo Wang<sup>1,2</sup>✉

## Abstract

This paper reports a high performance co-oscillating electrochemical vector hydrophone based on integrated microelectrodes with microgrooves. Through theoretical and simulation analysis, the influence of key parameters such as the spacing between anode and cathode, depth of microgrooves and the distribution of vias on the performance of the hydrophone was determined. By using the new microgroove structures, micron-scale anode and cathode spacing was realized and effective cathode areas were greatly enlarged and eventually increased the sensitivities of the hydrophones. Furthermore, a force-balanced negative feedback system was designed to expand the effective working band of the vector hydrophone. The characterization results indicated that the device had ~2 times higher original sensitivities and wider -3dB-bandwidth than that of existing devices. The above results show that the vector hydrophone developed in this work has a wide application scenarios in the field of underwater sound detections.

## Introduction

Vector hydrophones are essential transducers in underwater acoustic detection systems, widely used in marine research, resource development, and maritime military operations<sup>1</sup>. In particular, vector hydrophones offer a significant advantage in measuring the velocity and acceleration of sound vector field. This capability enhances their directional sensitivity and spatial resolution, which are critical for accurately detecting complex underwater soundscapes<sup>2</sup>.

The typical structure of a vector hydrophone is co-oscillating design, which is equipped with a vibration sensor to achieve synchronous vibration in response to acoustic signals. This design offers the advantages of small size and light weight<sup>3</sup>. So far, many efforts have been devoted to developing high-performance co-oscillating vector hydrophones based on various sensing mechanisms,

such as piezoresistive<sup>4–6</sup>, piezoelectric<sup>7–9</sup>, capacitive<sup>10,11</sup> and electrochemical effects. Among various devices, electrochemical co-oscillating vector hydrophone, utilizing electrolyte as liquid inertial mass block for vibration sensors, show great advantage of high sensitivity, wide frequency response and low mechanical noise, which is promising in underwater acoustic monitoring<sup>12</sup>. More importantly, since the electrochemical reaction is more sufficient at low frequency, electrochemical co-oscillating vector hydrophone can effectively monitor very low-frequency underwater acoustic signals below 20 Hz, offering excellent low-frequency performance compared to devices based on the other three principles<sup>13</sup>.

Co-oscillating electrochemical vector hydrophone is mainly composed of electrolyte solution and sensitive microelectrodes. The sensitive microelectrode is crucial to the noise suppression and frequency response of the electrochemical vector hydrophone<sup>14</sup>. Since Zhong et al. first employed MEMS electrochemical vibration sensor as the core vibrator of co-oscillating vector hydrophone<sup>15</sup>, various sensitive microelectrode structures, such as laminated electrodes structure, S-type electrodes structure and so on, had been explored to improve the

Correspondence: Yulan Lu (luy@aircas.ac.cn) or Deyong Chen (dychen@mail.ie.ac.cn) or Junbo Wang (jbwang@mail.ie.ac.cn)

<sup>1</sup>State Key Laboratory of Transducer Technology, Aerospace Information Research Institute, Chinese Academy of Sciences, Beijing, China

<sup>2</sup>School of Electronic, Electrical and Communication Engineering, University of Chinese Academy of Sciences, Beijing, China

© The Author(s) 2025



**Open Access** This article is licensed under a Creative Commons Attribution-NonCommercial-NoDerivatives 4.0 International License, which permits any non-commercial use, sharing, distribution and reproduction in any medium or format, as long as you give appropriate credit to the original author(s) and the source, provide a link to the Creative Commons licence, and indicate if you modified the licensed material. You do not have permission under this licence to share adapted material derived from this article or parts of it. The images or other third party material in this article are included in the article's Creative Commons licence, unless indicated otherwise in a credit line to the material. If material is not included in the article's Creative Commons licence and your intended use is not permitted by statutory regulation or exceeds the permitted use, you will need to obtain permission directly from the copyright holder. To view a copy of this licence, visit <http://creativecommons.org/licenses/by-nc-nd/4.0/>.

performance of electrochemical vibration sensor<sup>16–20</sup>. However, these microelectrode structures have limited effectiveness in improving the sensitivity of co-oscillating electrochemical vector hydrophones due to uncontrollable anode and cathode spacing and limited cathode area. Additionally, their high cutoff frequency is low, which restricts their ability to detect broadband underwater acoustic signals in low frequency band.

In this paper, we built the model through theoretical analysis and numerical simulation. The influence of key electrochemical microelectrodes parameters: spacing between anode and cathode, depth of microgrooves, via spacing and via diameter on the sensitivity was analyzed, and the key parameters of the microelectrodes were obtained. A novel micro-electrodes chip, utilizing microgrooves, was fabricated to achieve micron-scale anode and cathode spacing and larger effective cathode, significantly enhancing original peak sensitivity to  $-174.87$  dB(REF 0 dB=1 V/ $\mu$ Pa). To expand the bandwidth, a negative feedback system was introduced into the electrochemical vector hydrophone for the first time. As a result, the electrochemical vector hydrophone achieved a wider 3 dB bandwidth of 1–450 Hz, with sensitivity after negative feedback remaining around  $-183$  dB(REF 0 dB=1 V/ $\mu$ Pa). The above results show that the vector hydrophone proposed in this paper has a wide application scenario in the field of underwater sound.

## Materials and methods

### Working mechanisms and structures

Figure 1a shows the structural diagram of the co-oscillating electrochemical vector hydrophone, which mainly consists of a MEMS electrochemical vibration sensor and feedback system enclosed in a watertight and pressure-resistant package. The electrochemical vibration sensor integrates micro-electrodes based on deep microgrooves and an electrolyte liquid system of iodine and potassium iodide.

Figure 1b shows the sensitivity principle of the co-oscillating electrochemical vector hydrophone, where redox reaction pairs  $3I^- - 2e^- \rightarrow I_3^-$  and  $I_3^- + 2e^- \rightarrow 3I^-$  occur on the anode and cathode of the micro-electrodes respectively. When there is no disturbance of external sound field, the ion concentration gradient between anode and cathode tends to be stable. When the external sound field is applied to the co-oscillating electrochemical vector hydrophone, the hydrophone will vibrate at the sound particle vibration velocity, causing convective movement of the electrolyte. This movement alters the ion concentration gradient between the anode and cathode. The concentration gradients of both anode-cathode pairs change equally but in opposite directions, resulting in opposite output current changes from the two cathodes.

The output current difference between the two cathodes is calculated and converted into a voltage, and finally an output voltage related to the external sound particle vibration velocity is obtained. The difference in output current between the two cathodes is then calculated and converted into a voltage, resulting in an output voltage that is related to the external sound particle vibration velocity.

The MEMS micro-electrodes proposed in this paper integrate four electrodes (anode-cathode-cathode-anode) on a single silicon chip, as shown in Fig. 1c. Deep microgrooves are used to isolate the anode and cathode, with the channel width precisely controlled at the micron level, resulting in an improvement in original sensitivity.

Meanwhile, as the original 3 dB bandwidth of MEMS electrochemical vector hydrophones is relatively narrow. Negative feedback is commonly employed to expand the bandwidth, but this approach will sacrifice some sensitivity. This paper presents a force-balancing negative feedback system based on a coil and magnet, as illustrated in Fig. 1a. The feedback voltage ( $U_f$ ) is applied to the feedback coil (with length  $L_{coil}$  and resistance  $R_{coil}$ ), generating a current ( $I_f$ ). The magnetic field ( $B$ ) of the feedback magnet interacts with the energized coil, producing an Ampere force ( $F_f$ ), which serves as the feedback force.

### Theoretical and simulation model analysis

More specifically, the energy exchange process of the co-oscillating electrochemical vector hydrophone can be divided into three processes: acoustic-to-vibration conversion, vibration pickup, and electrochemical-mechanical conversion<sup>15</sup>.

In the process of acoustic-vibration conversion, the sound particle vibration velocity  $V_0$  is converted into the overall vibration velocity  $V$  of the hydrophone. This paper proposes a cylindrical hydrophone. When the size of the cylinder is much smaller than the wavelength ( $ka \ll 1$ , where  $k$  is the wave number and  $a$  is the maximum size of the cylinder), the  $V_0$ ,  $V$  and their phase difference  $\theta$  meet the following relation<sup>21</sup>:

$$\frac{V}{V_0} = \frac{2\rho_0}{\rho + \rho_0}, \theta \rightarrow 0 \quad (1)$$

where  $\rho_0$  is the density of water and  $\rho$  is the overall average density of hydrophone. When the density of hydrophone and water are consistent, it can realize the lossless and phase-shift-free conversion from sound particle vibration velocity  $V_0$  to the vibration velocity  $V$  of the vector hydrophone.

The vibration pickup process describes the conversion process from the overall vibration velocity  $V$  of the hydrophone to the flow velocity  $v$  of the electrolyte near

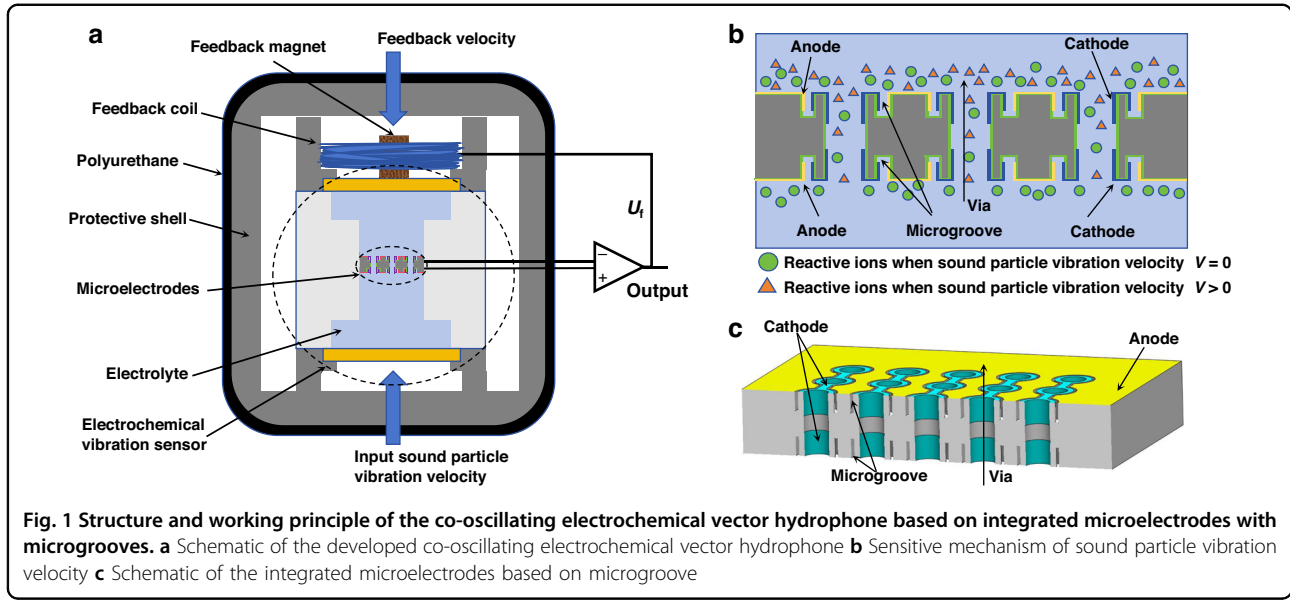


**Fig. 1** Structure and working principle of the co-oscillating electrochemical vector hydrophone based on integrated microelectrodes with microgrooves. **a** Schematic of the developed co-oscillating electrochemical vector hydrophone **b** Sensitive mechanism of sound particle vibration velocity **c** Schematic of the integrated microelectrodes based on microgroove

the micro-electrodes. It is a second-order spring-mass-damping system, whose transfer function can be expressed as<sup>22</sup>:

$$\left| \frac{v(w)}{V(w)} \right| = \frac{w^2}{\sqrt{(w^2 - w_0^2)^2 + R_e^2 w^2}} \quad (2)$$

Where  $w_0$  is the natural frequency of the system and  $R_e$  is the equivalent flow resistance of the system, which has the following relationship with the number of vias  $n$  and the radius of vias  $r_v$ , according to Poiseuille law<sup>22</sup>:

$$R_e \sim \frac{1}{nr_v^4} \quad (3)$$

It can be seen that the above transfer function represents a high-pass model, where the low-frequency cutoff increases with the flow resistance  $R_e$  increasing.

The electrochemical-mechanical conversion process describes the conversion process of the fluid velocity  $v=v_a \sin(2\pi f_0 t + \beta)$  of the electrolyte near the microelectrodes to the differential current  $I$  of the two cathodes of the micro-electrodes. The output cathode current  $I$  can be expressed in terms of Faraday's law:

$$I = qF \int_s J \bullet m ds \quad (4)$$

Where  $q$  is the number of electrons exchanged in the cathode reaction,  $F$  is the Faraday constant,  $s$  is the effective electrode area of the cathode,  $m$  is the normal vector of the cathode surface and  $J$  is the reactive ion flux.

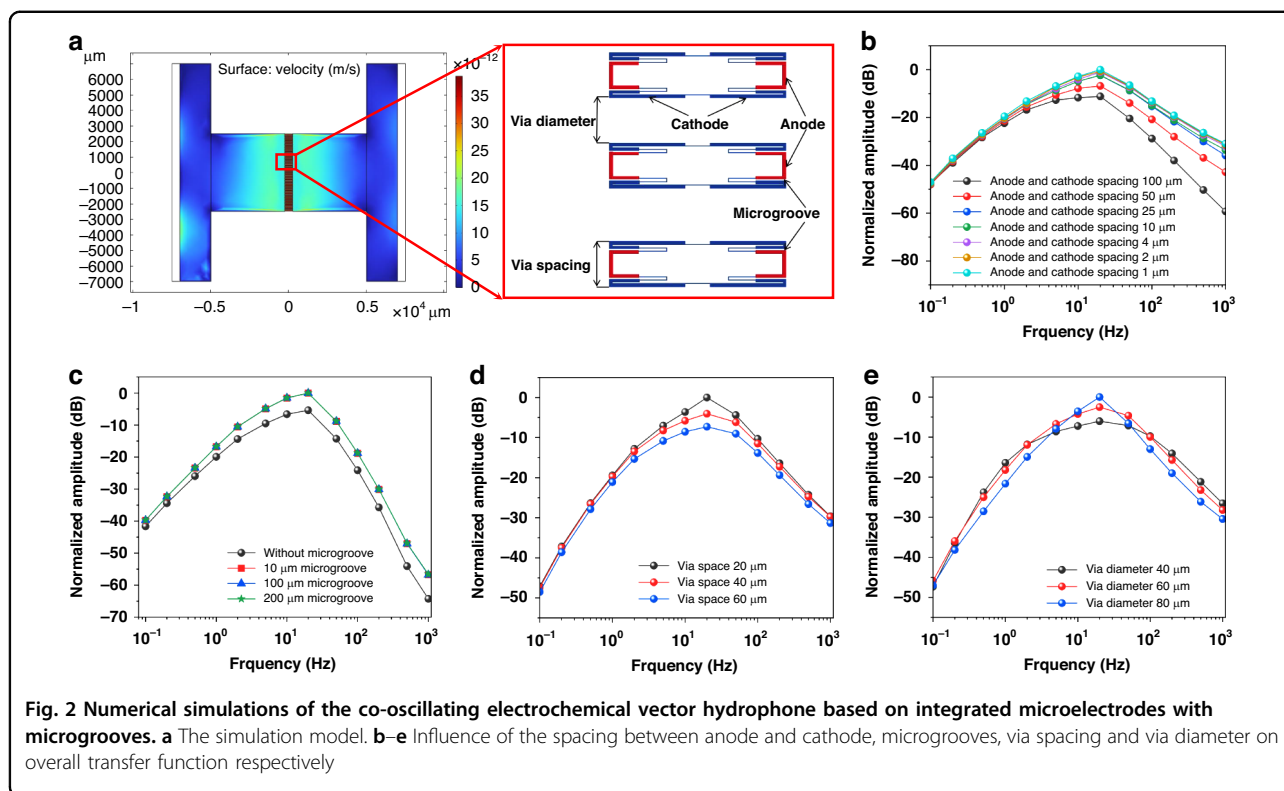
$J$  can be obtained from the Nernst-Planck equation:

$$J = -D\nabla C - \frac{zF}{RT} DC\nabla\phi + Cv \quad (5)$$

Where  $v$  is the flow velocity of the electrolyte near the microelectrodes,  $C$  is the reactive ion concentration,  $z$  is the number of charges carried by the ion,  $R$  is the gas constant,  $T$  is the absolute temperature,  $\phi$  is the electric potential, and  $D$  is the diffusion coefficient. It can be seen from formula (5) that the flux of reactive ions  $J$  is composed of three parts: diffusion, electromigration and convection. When there's no acoustic signal, the  $J$  is mainly composed of diffusion and electromigration. For the two cathodes symmetrically distributed in the microelectrode, their effective electrode areas and the normal vector on the cathode surface are same. Consequently,  $J$  is also equal, resulting in zero differential cathode current. When the vector hydrophone detects a sound wave, convection occurs near the microelectrode, dominating the reactive ion flux  $J$ . The analytical solution is obtained by determining the electrolyte flow velocity near the microelectrodes  $v$  and the reactive ion concentration  $C$ . After simplified calculation of  $C$  and  $v$ , the final cathode differential output current can be expressed as<sup>20</sup>:

$$I = \frac{qFs}{2\pi f_0 L} v_a \sin(2\pi f_0 t + \beta) \quad (6)$$

Where  $L$  is the spacing between anode and cathode. From formula (6), it can be seen that the output cathode current increases with the increase of cathode area  $s$  and the decrease of anode and cathode spacing  $L$ . As the



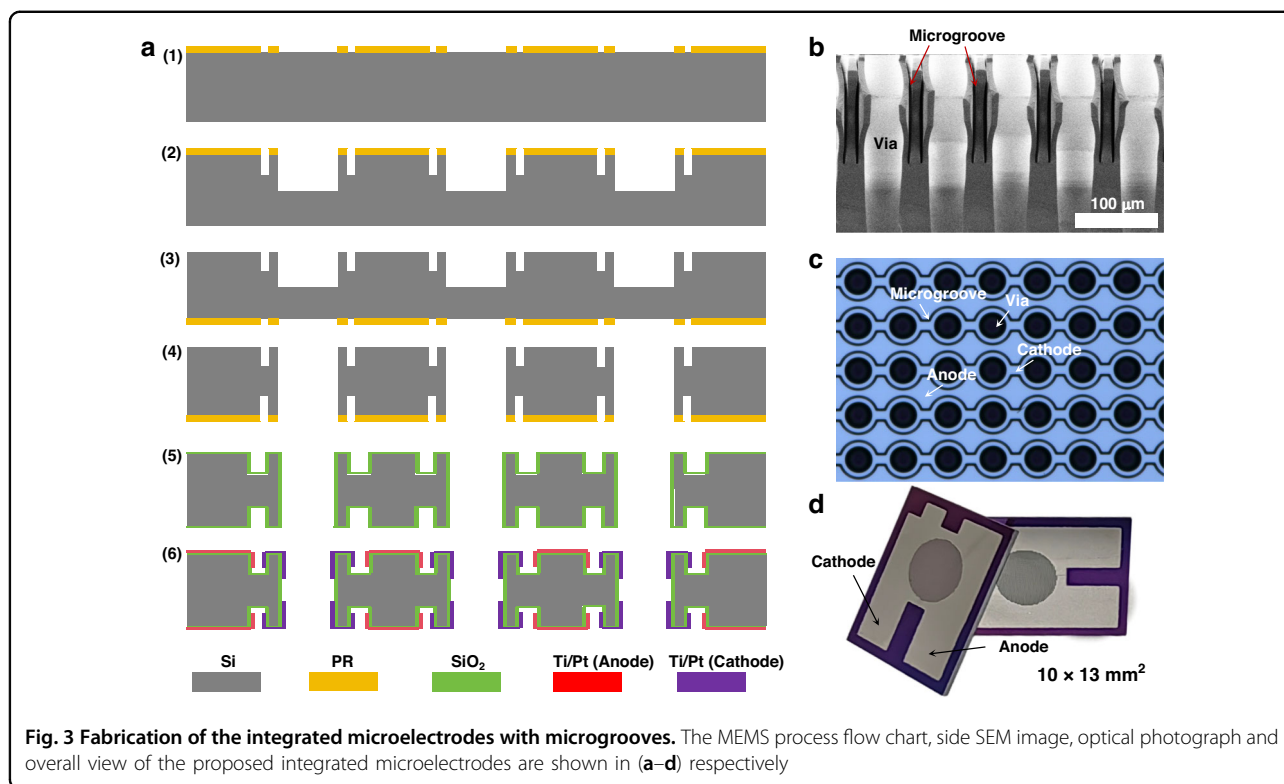
frequency increases, the output current decreases. Thus the electrochemical-mechanical conversion process indicates a low-pass characteristic and in summary, the overall transfer function presents a band-pass.

Based on the above model, the influence of key parameters on the performance of vector hydrophone was studied through numerical simulation. Specifically, solid mechanics and laminar flow multiphysics fields are used for the vibration pickup process, while laminar flow and tertiary current distribution multiphysics fields are applied in the electrochemical-mechanical conversion process. The established specific models are shown in Fig. 2(a), where the influence of key parameters, including spacing between anode and cathode, the depth of microgroove, via spacing and via diameter on the output amplitude was explored.

Figure 2b shows the effect of the spacing between anode and cathode (the width of microgrooves) on the over-all transfer function. It can be seen that the output indicates a band-pass characteristic. At frequencies above 1 Hz, the output amplitude increases significantly as the spacing between the cathode and anode reduces. When the spacing is reduced to below 4  $\mu\text{m}$ , further improvement is negligible, because the electrochemical reaction rate between the anode and cathode has reached saturation. Therefore, micron-scale anode and cathode spacing is necessary for high sensitivity. Meanwhile, the influence of microgrooves on the performance of the hydrophone was

investigated, as shown in Fig. 2c. The depths of the microgrooves at the anode-cathode spacing are 0, 10 100 and 200  $\mu\text{m}$ , respectively. It can be seen that the sensitivity of the hydrophone is significantly improved by setting microgrooves between the anode and cathode. But as the microgrooves get deeper, the sensitivity of hydrophone has almost no change, which indicates that microcontrolling the anode-cathode spacing by microgrooves will not affect the dynamic performance of the hydrophone. This is because microgrooves introduce additional cathodes in its side walls, resulting in more reactive ion flux, as shown in Figure S1. However, due to the inability of the deeper regions of the microgrooves to generate convective disturbance of the electrolyte, deeper microgrooves do not further enhance sensitivity. From the above simulation results, the design of the microgroove structure reduces the anode-cathode spacing on one hand and increases the effective cathode area on the other hand, serving as an effective method to enhance sensitivity.

Figure 2d and e shows the influence of the via diameter and via spacing on hydrophone sensitivity, respectively. The results indicate that a smaller via diameter enhances high-frequency sensitivity and expands the bandwidth, but reduces peak sensitivity. The via spacing primarily affects both peak sensitivity and bandwidth, with smaller spacings leading to higher peak sensitivity but a narrower bandwidth. This is because a smaller diameter increases



flow resistance and the cathode area, leading to the turning point of the vibration pickup process moving to higher frequency and the overall improvement of the output of the electrochemical-mechanical conversion process. While small spacing decreases flow resistance and increases the cathode area, leading to the turning point of the vibration pickup process moving to lower frequency and the overall improvement of the output of the electrochemical-mechanical conversion process, as shown in Fig. S2. Therefore, the anode-cathode spacing, via diameter, and via spacing are critical for improving the sensitivity and bandwidth of the hydrophone and should be considered in the design of the microelectrode structure.

#### Design and fabrication of the microelectrodes

Based on the above theoretical simulation analysis, the key parameters for anode-cathode spacing, via diameter, and via spacing are determined. An electrochemical microelectrode chip is then fabricated using the MEMS process. The fabrication steps are shown in Fig. 3a.

1. The vias and microgrooves were patterned by using lithography on the front side of the double-polished Si wafer with a thickness of 510  $\mu\text{m}$ . The width of the microgrooves, corresponding to anode-cathode spacing, is 4  $\mu\text{m}$ . The vias diameter is 60  $\mu\text{m}$ , and the vias spacing is 30  $\mu\text{m}$ , 40  $\mu\text{m}$ , 50  $\mu\text{m}$  and 60  $\mu\text{m}$ , respectively.

2. Deep reactive ion etching (DRIE) technology is used to achieve deep etching of vias and microgrooves on the front side of the wafer. Since the via diameter is 60  $\mu\text{m}$ , much larger than the 4- $\mu\text{m}$ -wide microgrooves, owing to the Aspect Ratio Dependent Etching (ARDE), the vias are etched to a depth of 255  $\mu\text{m}$ , while the microgrooves etching is stopped at 100  $\mu\text{m}$ .
3. On the back side of wafer, the vias and microgrooves were prepared by using lithography and DRIE process, with the same size and mirroring position that of the front side. The etching depth of vias on the back side is 255  $\mu\text{m}$ , indicating that the vias have been fully etched. Furthermore, similarly as the front side, the etching of microgrooves is stopped at the depth of 100  $\mu\text{m}$ .
4. A 1- $\mu\text{m}$  thick  $\text{SiO}_2$  insulating layer is grown across the entire wafer through the thermal oxidation process.
5. Two pairs of electrodes were defined using a hard mask, and Ti/Pt metal layers (30/250 nm) were deposited on the front and back sides of the wafer using a magnetron sputtering process (taking advantage of the directionality of sputtering process) to form cathode and anode electrodes.

Figure 3b shows a side SEM image of the microelectrodes chip, where the vias are fully etched and the microgroove depth is approximately 100  $\mu\text{m}$ . Figure 3c

shows an optical photograph of the microelectrodes, where microgrooves surround the vias, and the anode and cathode are separated evenly by the microgrooves. The microgroove design not only reduces the spacing between the cathode and anode to improve the efficiency of electrochemical reaction, but also significantly reduces manufacturing complexity compared to previous microelectrodes<sup>16–20</sup>.

## Result

In order to expand the pass band, an additional force-balancing negative feedback process was introduced, whose whole closed-loop transfer function block diagram is shown in Fig. S2. The circuit system mainly includes signal conditioning circuit part and feedback circuit part. The conditioning circuit is used to implement transresistance and difference operations. Feedback circuit is used to convert the feedback acceleration signal to speed signal and to control the feedback strength. By adjusting the resistance  $r$ , the overall closed-loop transfer function can exhibit a flat passband. As  $r$  increases, the feedback strength and passband width also increase, but sensitivity is sacrificed accordingly.

The microelectrode and feedback system were successfully encapsulated into an electrochemical vibration sensor and placed within a protective shell. The sensor was then sealed with polyurethane and assembled into a co-oscillation MEMS electrochemical vector hydrophone, as shown in Fig. 4a. The encapsulated hydrophone has a cylindrical shape, with a diameter of 25 mm and a height of 60 mm. To investigate the performance of the hydrophone, a custom-designed test platform was built, including a standard vibration table and standing-wave tube, as shown in Fig. 4a. More specifically, the sensitivity curve of 20–500 Hz was calibrated in the standing-wave tube at a depth of 20 cm with a standard hydrophone to calculate the sound particle vibration velocity. Since the standing-wave tube cannot emit low frequency acoustic standing-wave below 20 Hz, using vibration table to calibrate the sensitivity curve of 0.7 Hz–500 Hz. The directivity curve was calibrated in standing-wave tube.

Figure 4b shows the sensitivity curves of the hydrophone with different design of via spacing of 30, 40, 50, and 60  $\mu\text{m}$ . It can be seen that the larger the via spacing, the lower the sensitivity of the hydrophone, which matches well with the theoretical simulation in Fig. 3d. The device with a 30- $\mu\text{m}$  via spacing exhibits a higher peak sensitivity of -174.87 dB (REF 0 dB=1 V/ $\mu\text{Pa}$ ) at 30 Hz. Figure S3 shows the sensitivity of three hydrophones with a spacing of 40  $\mu\text{m}$ . The three curves nearly overlap, indicating that the electrochemical hydrophone exhibits excellent consistency.

Figure 4c is a comparison of the sensitivity and bandwidth before and after the negative feedback system is

applied. The bandwidth was extended through the negative feedback system from 20–100 Hz to 1–450 Hz, and the sensitivity of the hydrophone remained at around -183 dB (REF 0 dB=1 V/ $\mu\text{Pa}$ ). Meanwhile, the sensitivity results tested in the standing-wave tube are consistent with the sensitivity results tested on the vibration table.

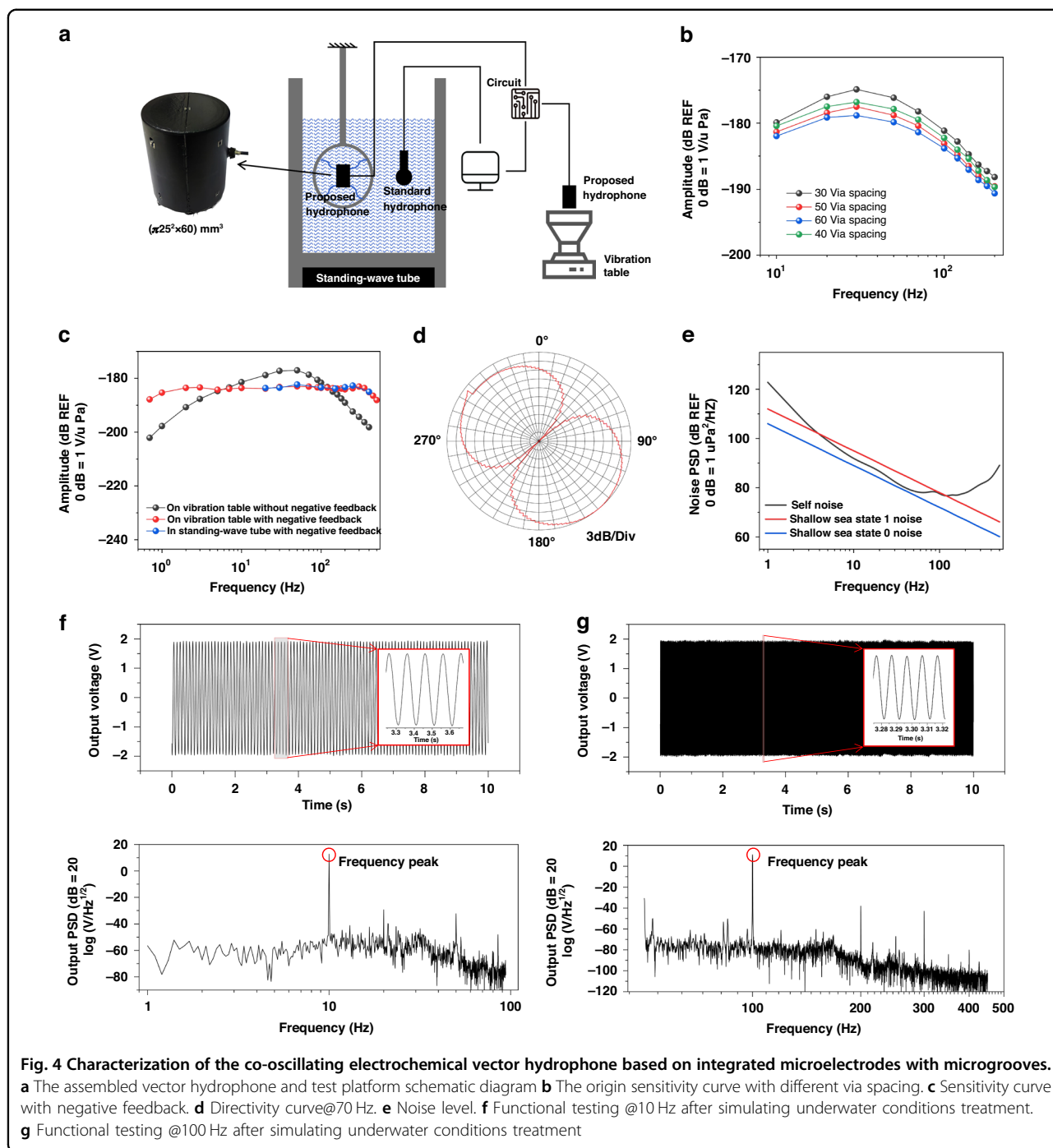
The directivity curve of the vector hydrophone were measured at the frequency of 70 Hz, as shown in Fig. 4d. The test results show that the novel electrochemical vector hydrophone possesses directional pattern in the form of “8” shape, and the depth of the concave point reaches -40.6 dB. The “8” shaped directivity curve is smooth, and the maximum non-uniformity of the axial sensitivity is 1.9 dB.

Figure 4e shows the noise level of proposed vector hydrophone, which is approximately near the shallow sea self-noise level in ocean state 0 at low frequency, with 78.658 dB compared with ocean state 0 self-noise level 77.9 dB<sup>21</sup> at 50 Hz, and is strictly below the shallow sea state 1 noise within the frequency range of 4–140 Hz.

Stability and reliability test under harsh underwater conditions was conducted by applying a pressure of 2 Mpa (Pressure at a water depth of 200 meters) to the vector hydrophone for 30 minutes through a pressure tank and immersing the vector hydrophone in simulated seawater (salinity 30%, pH = 8.5, containing NaCl and Na<sub>2</sub>CO<sub>3</sub>). Post-test inspection confirmed no structural deformation. Subsequent functional testing validated its working performance. The vector hydrophone was subjected to excitation signals of 2 mm/s at 10 Hz and 100 Hz. The device maintained undistorted time-domain signal output and exhibited distinct frequency peaks at 10 Hz and 100 Hz in the frequency domain, as illustrated in Fig. 4f and g. The above results indicate that the described vector hydrophone operates effectively under harsh underwater environments at depths up to 200 meters.

Table 1 compares the original sensitivity of different electrochemical vibration sensor of the vector hydrophone. It shows that our device has higher sensitivity over the entire tested frequency band. Most prominently, the peak sensitivity has been improved by about two times compared to the current best level (-174.87 dB vs. -180.30 dB REF 0 dB=1V/ $\mu\text{Pa}$ ). This boost is because our microelectrodes have smaller anode-cathode spacing and larger effective cathode area with the design of microgrooves, enhancing the electrochemical reaction capacity.

Table 2 compares this work with prominent vector hydrophones. It shows that our device exhibits high sensitivity of -183 dB (REF 0 dB=1V/ $\mu\text{Pa}$ ) and a wider 3 dB bandwidth of 1-450 Hz compared to the existing co-vibration electrochemical vector hydrophone and the increase of sensitivity at higher frequency is conducive to the improvement of high cutoff frequency after feedback.



**Table 1 Comparison of the original sensitivity of different electrochemical vector hydrophones at different frequency**

Device	Sensitivity@1 Hz	Peak sensitivity	Sensitivity@200 Hz
This study	-197.73 dB (194.31 V/(m/s))	-174.87 dB@30 Hz (2700.85 V/(m/s))	-188.15 dB (585.46 V/(m/s))
A. Zhong <sup>15</sup>	-214dB (30 V/(m/s))	-188.86 dB@80 Hz (563.44 V/(m/s))	-193dB (335 V/(m/s))
L. Hu <sup>23</sup>	-206dB (75 V/(m/s))	-180.30 dB@90 Hz (1445.44 V/(m/s))	-190dB (473 V/(m/s))

dB REF 0 dB=1 V/μPa;  
 Following is the equivalent vibration velocity sensitivity of the core vibration sensor.

**Table 2 Comparison of the final characteristic of different vector hydrophones**

Device	Sensitivity@10 Hz	Sensitivity@200 Hz	−3dB bandwidth
This study	−183.5 dB	−183.5 dB	1–450 Hz
Electrochemical <sup>15</sup>	−187dB	−193dB	0.5–150 Hz
Electrochemical <sup>23</sup>	−180dB	−190dB	0.8–100 Hz
Piezoresistive <sup>4</sup>	/	−190dB	/
Piezoelectric <sup>7</sup>	−230dB	−207dB	/
Capacitive <sup>10</sup>	/	−194.5 dB	/

dB REF 0 dB=1 V/μPa

Moreover, our electrochemical hydrophone demonstrates high sensitivity at low frequency, outperforming the other three types of hydrophones. These results suggest that our device holds significant potential for applications in underwater acoustic target detection, sonar systems, and unmanned underwater vehicles.

## Conclusions

This study introduces design, fabrication, and characterization of a new co-oscillating electrochemical vector hydrophone with high performances in low frequency bandwidth. A new microgrooves-based integrated micro-electrodes and a negative feedback mechanism was employed in the electrochemical vector hydrophones for the first time. The test results shown that the developed hydrophone had high sensitivities, directivities and noise performances. Most importantly, it realized a high-sensitive underwater acoustic detection with wider 3 dB bandwidth in the low frequency bandwidth, which is difficult for other vector hydrophones to achieve, showing its application prospect in the field of underwater acoustic detections.

## Acknowledgements

This study was supported in part by the Strategic Priority Research Program (B) of the Chinese Academy of Sciences under Grant XDB1110201, in part by the National Natural Science Foundation of China under Grant 62201549, Grant 52335012, and Grant U23A20362, in part by Beijing Natural Science Foundation under Grant 4242012, in part by the Youth Innovation Promotion Association CAS under Grant 2023134.

## Author contributions

Yulan Lu, Junbo Wang and Deyong Chen supported and conceived the experiments and correspondence to this article; Honghao Zhang performed the numerical simulations and the experiments, as well as most of the analysis, data acquisition and processing, and writing; Lintao Hu, Qinghua Liu, Wenlang Zhao, Hongmin Jiang, Maoqi Zhu and Zhenyu Sun contributed to parts of the analysis and discussion; Guangyang Gou contributed to parts of the analysis and polishing of the article.

## Competing interests

The authors declare no competing interests.

**Supplementary information** The online version contains supplementary material available at <https://doi.org/10.1038/s41378-025-01040-z>.

Received: 7 May 2025 Revised: 15 July 2025 Accepted: 7 August 2025

Published online: 12 November 2025

## References

- Chen, L., Zhang, P., Xu, X. & Wang, F. Overview of vector hydrophone. *Transducers Microsyst. Technol.* **25**, 5–8 (2006).
- Saheban, H. & Kordrostami, Z. Hydrophones, fundamental features, design considerations, and various structures: A review. *Sens. Actuat. A Phys.* **329**, 112790 (2021).
- Ding, R., Tang, J., Zhao, Z. & Fan, M. Domestic research status and future technology development of MEMS hydrophone. *Transducers Microsyst. Technol.* **41**, 157–160 (2022).
- Zhang, X. et al. Design and implementation of anulus-shaped ciliary structure for four-unit MEMS vector hydrophone. *Int. J. Metrol. Qual. Eng.* **12**, 4 (2021).
- R. Wang et al. Design and implementation of a jellyfish otolith-inspired MEMS vector hydrophone for low-frequency detection. *Microsyst. Nanoeng.* **7**, (2021).
- Ren, W. et al. Design and implementation of Crossed-circle MEMS ciliary vector hydrophone. *Measurement* **201**, 111678 (2022).
- Fan, Q., Li, J., Zhai, Y. & Ma, J. A novel MEMS piezoelectric vector hydrophone. *Acta Acust.* **48**, 102–111 (2023).
- Ganji, B. A., Nateri, M. S. & Dardel, M. Design and modeling of a novel high sensitive MEMS piezoelectric vector hydrophone. *Microsyst. Technol.* **24**, 2085–2095 (2018).
- Shi, S. et al. Design and fabrication of a novel MEMS piezoelectric hydrophone. *Sens. Actuator A Phys.* **313**, 112203 (2020).
- Gong, Z. et al. Novel tri-axial MEMS capacitor vector hydrophone. *J. CAEIT* **8**, 205–208 (2013).
- Zhang, Y., Gui, C. & Li, X. Research on silicon micro capacitive one-dimensional vector hydrophone. *Appl. IC* **35**, 54–56 (2018).
- Krishtop, V. G., Agafonov, V. M. & Bugaev, A. S. Technological principles of motion parameter transducers based on mass and charge transport in electrochemical microsystems. *Russ. J. Electrochem.* **48**, 746–755 (2012).
- Huang, H., Agafonov, V. & Yu, H. Molecular electric transducers as motion sensors: a review. *Sensors* **13**, 4581–4597 (2013).
- Egorov, E. V., Egorov, I. V. & Agafonov, V. M. Self-noise of the MET angular motion seismic sensors. *J. Sens.* **2015**, 1–5 (2015).
- Zhong, A. et al. A MEMS-based co-oscillating electrochemical vector hydrophone. *Micromachines* **13**, 143 (2022).
- Qi, W. et al. MEMS-based electrochemical seismometer with a sensing unit integrating four electrodes. *Micromachines* **12**, 699 (2021).
- He, W. et al. Low frequency electrochemical accelerometer with low noise based on MEMS. *Key Eng. Mater.* **503**, 75–80 (2012).
- Liang, T. et al. A micromachined electrochemical angular accelerometer with highly integrated sensitive microelectrodes. *Microsyst. Nanoeng.* **8**, 100 (2022).
- Liu, B. et al. A new electrochemical angular microaccelerometer with integrated sensitive electrodes perpendicular to flow channels. *Microsyst. Nanoeng.* **8**, 80 (2022).

20. Deng, T. et al. A MEMS based electrochemical vibration sensor for seismic motion monitoring. *J. Microelectromech Syst.* **23**, 92–99 (2014).
21. Zhang, H. *Research on Hot-wire MEMS Vector Hydrophone with Enhanced Sensitivity Structure*. (China Jiliang University, 2018).
22. Xu, C. *Study on MEMS Based Electrochemical Seismic Sensors with High Sensitivity and Wide Bandwidth for Deep-Sea Exploration* (University of Chinese Academy of Sciences, 2021).
23. Hu, L. et al. A very low-frequency 3-D vector hydrophone based on an electrochemical vibration sensor. *IEEE Sens. J.* **25**, 14709–14716 (2025).